

Investigating the Kinetic Effects on Current Gradient-Driven Instabilities of Electron Current Layers via Particle-in-Cell Simulations

Sushmita Mishra,¹ Gurudatt Gaur,^{2,3} and Bhavesh G. Patel⁴

¹*Institute of Advanced Research, Koba Institutional Area, Gandhinagar 382 426, India*

²*St. Xavier's College (Autonomous), Navrangpura, Ahmedabad 380 009, India*

³*Kshama Ahmedabad Academy of Sciences, Motera, Ahmedabad 380 005, India*

⁴*Institute for Plasma Research, Bhat, Gandhinagar 382 428, India*

(*Electronic mail: gurudatt.gaur@sxca.edu.in)

(*Electronic mail: mishra.sushmita0@gmail.com)

(Dated: 10 July 2024)

Electron current layers form in various natural and laboratory plasmas and are susceptible to several instabilities. Tearing, driven by current gradients, stands out as a prominent instability in these layers and is considered a potential mechanism for magnetic reconnection in collisionless regimes. Electron inertia serves as a non-ideal factor causing magnetic field lines to break and subsequently reconnect. Another mode driven by current gradients, known as the surface-preserving mode, maintains magnetic field topology. We investigated the kinetic effects on these modes in the presence of finite electron temperatures using two-dimensional particle-in-cell simulations (implemented with the OSIRIS codebase). Temperature stabilizes the tearing mode to a large extent, except at low temperatures, due to increased electron Larmor radius and subsequent magnetic field diffusion. Introducing uniform guide fields revealed that growth rates decrease at higher temperatures due to reduced plasma beta. Conversely, for the surface-preserving mode, growth rates increase with temperature, likely due to enhanced electron flow velocities. Mixed modes, where both tearing and surface-preserving modes coexist, exhibit asymmetric structures characteristic of asymmetric magnetic reconnection. Finally, we propose future research directions building upon our findings.

I. INTRODUCTION:

Plasma is a state of matter in which electrons and ions move freely, exhibiting collective behavior under the influence of electric and magnetic fields produced either by their own motion or by external sources. Studying plasma properties is essential for understanding various natural phenomena and for advancing technological applications. This research often involves measurements on natural plasmas and sophisticated laboratory experiments to study plasma behavior under different conditions.

Magnetic fields significantly influence plasma dynamics, leading to rich and complex behaviors. They affect the motion of charged particles, which in turn modify the magnetic fields due to the frozen-in condition arising from the high electrical conductivity of plasmas. One key phenomenon where the magnetic field is altered by plasma particles is magnetic reconnection (MR). In MR, plasma pushes two oppositely directed magnetic field lines towards each other, changing the topology of the magnetic field lines.¹ MR is observed in various natural settings, including the solar system. It plays a crucial role in solar flares, coronal mass ejections, the Earth's magnetosphere, and astrophysical jets. MR is also believed to occur during star formation. Additionally, MR is observed in several fusion plasma devices, such as Tokamak, Reverse Field Pinch, and Spheromak. Numerous laboratory plasma devices have been created to understand the mechanisms behind MR.²⁻⁴

Significant efforts have been made to propose theoretical models explaining MR at different time and length scales in various plasma conditions. The Sweet-Parker model, independently proposed by Sweet and Parker, is one of the ear-

liest models describing magnetic reconnection. This resistive MHD (magnetohydrodynamics) model describes reconnection occurring in a long, narrow current sheet with a reconnection rate limited by plasma resistivity.⁵ However, this model predicts a slow reconnection rate, insufficient to explain the fast reconnection events observed in nature.⁶ The Petschek model, introduced by Petschek, suggests a faster reconnection process facilitated by standing slow-mode shocks forming at the edges of a much shorter and wider diffusion region with localized regions of enhanced resistivity, allowing rapid conversion of magnetic energy. However, this model assumes a certain level of collisionality and is less applicable to collisionless plasmas.⁷ Space and astrophysics plasmas, where fast reconnection occurs, are known to be collisionless. In a collisionless plasma, where the mean free path of particles is much larger than the system size, the reconnection dynamics is predominantly governed by the electromagnetic forces rather than collisional interactions.

Various models have been proposed to understand fast reconnection in collisionless plasmas, addressing different aspects and scales of the process, both fluid and kinetic. While the MHD model is valuable for understanding large-scale plasma behavior, it is insufficient for describing the detailed physics of collisionless MR. For collisionless plasmas, models which include electron scale dynamics such as EMHD (electron magnetohydrodynamics)⁸, Hall MHD, and two-fluid MHD,⁹⁻¹² or the models that include kinetic effects, such as hybrid¹³ and full kinetic (PIC: particle-in-cell) models,^{14,15} are necessary to accurately capture the complex dynamics and fast reconnection rates observed in these environments. These models incorporate the Hall term and electron inertia, leading to faster reconnection rates and more complex magnetic

island structures than single-fluid MHD models can provide.

Hall MHD, a subset of two-fluid models, specifically includes the Hall term, representing the differential motion between ions and electrons. This model has been pivotal in explaining fast reconnection rates and the formation of fine structures within the reconnection layer. Mandt et al. investigated the transition from resistive MHD reconnection to Hall MHD reconnection and emphasized the role of whistler waves in two-fluid models.¹⁶ The study illustrated how the Hall term becomes important at scales smaller than the ion inertial length, leading to faster reconnection rates. Shay et al. used two-fluid simulations to study the structure of the dissipation region during collisionless reconnection.¹⁰ The results highlighted the importance of the Hall effect and electron inertia in creating fast reconnection rates and forming magnetic islands. Rogers et al. examined the role of dispersive waves, such as whistler and kinetic Alfvén waves, in collisionless MR using Hall MHD simulations.¹⁷ They demonstrated how these waves contribute to the fast reconnection process and the development of tearing instability. Wang et al. investigated the scaling properties of collisionless reconnection in the presence of a strong guide field using two-fluid simulations.¹⁸ Birn et al. compared various simulation approaches, including two-fluid models, for studying MR.¹⁹ Their study highlighted the differences in reconnection rates and layer structures between different models. The study discussed how the tearing instability evolves and leads to fast reconnection rates in such configurations. Huba et al., provided a comprehensive overview of Hall MHD, including its application to MR, discussing how the inclusion of the Hall term leads to faster reconnection rates and the formation of magnetic islands.²⁰ Drake et al. provided a detailed analysis of the Hall fields' role in fast MR using two-fluid simulations¹¹. They explored how the Hall effect and electron inertia lead to the formation of magnetic islands and enhance the reconnection rate.

Particle-in-cell (PIC) simulations provide a more detailed approach by modeling individual particles and their interactions, capturing the full kinetic behavior of plasmas.²¹ PIC methods are particularly suited for investigating the microscale processes such as the formation of electron and ion diffusion regions, the development of current sheets, and the dynamics of magnetic islands. The electron diffusion region (EDR) is critical for collisionless reconnection, where electrons decouple from magnetic field lines. PIC simulations have revealed complex structures within the EDR, including crescent-shaped electron velocity distributions and the formation of electrostatic fields that facilitate reconnection.²² In the ion diffusion region (IDR), PIC simulations by Hesse et al., have highlighted the role of ion-scale structures and kinetic Alfvén waves in the reconnection process.²³ These simulations show how ion outflows and the development of Hall magnetic fields contribute to the overall dynamics of MR. The presence of a guide field (magnetic field component parallel to the reconnection plane) significantly influences the reconnection dynamics. Drake et al., via PIC simulations studies have demonstrated that guide fields can stabilize the current sheet, alter the structure of magnetic islands, and affect particle acceleration mechanisms.²⁴ Dahlin et al., in their

PIC simulations have identified multiple acceleration mechanisms, including direct acceleration by reconnection electric fields, Fermi acceleration in contracting magnetic islands, and betatron acceleration due to magnetic field compression.²⁵ While much of the initial work focused on two-dimensional (2D) models, recent advancements have emphasized the importance of three-dimensional (3D) effects in MR. Daughton et al. found that, compared to the single-X-line model, the multiple-X-line model is more compatible with the 3D PIC simulation.²⁶ Recently, 3D PIC simulations by Daughton et al., reveal complex structures such as flux ropes, turbulence, and the interaction between multiple reconnection sites, providing a more comprehensive understanding of reconnection in realistic settings.²⁷

A specific manifestation of magnetic reconnection (MR) is the tearing instability, which represents a dynamic approach to studying MR. Unlike the steady state approaches exemplified by the Sweet-Parker and Petschek models, the tearing instability involves the formation of a chain of magnetic islands and reconnection layers. This process leads to a reconfiguration of the magnetic topology. The tearing mode evolves according to parameters such as the width of the current sheet (ϵ) and the length scales characteristic of kinetic effects. These include the electron inertial skin depth (d_e), the ion inertial skin depth (d_i), and the Larmor radius of electrons or ions (r_L).¹² Tearing instability of thin current layers, of thickness smaller than the ion skin depth, has been studied by many researchers in the context of 2D and 3D EMHD.

EMHD model focuses on electron-scale dynamics by treating ions as a static background; whistler being the normal mode. Bulanov et al., provides exact self-similar solutions for EMHD, describing magnetic collapse and reconnection near singular points, showing the formation of current sheets and complex magnetic island structures.⁸ Subsequent work by Avinash et al. delved into forced magnetic field line reconnection within the framework of EMHD and utilized the approximation adopted in the theory of the tearing mode. Their analytic and numerical simulation results highlighted how the plasma and the magnetic field evolve over time when perturbations are imposed from the boundary of a high conductivity plasma slab, thus altering the topology of the magnetic field due to the effect of electron inertia.²⁸ Del Sarto et al., examined current layer cascade in collisionless EMHD reconnection, considering electron compressibility effects. The study investigated the importance of pressure-driven and inertia-driven dissipation mechanisms, showing that their dominance depends on the relative scaling of the electron thermal Larmor radius and electron inertia skin depth.²⁹ The study by Drake et al. explores the breakup of electron current layers with a scale length of d_e as a result of shear-flow instability during 3D collisionless MR under the EMHD regime. Moreover, it was noted that electron inertia is required to break the usual frozen flux constraint and suggests turbulent behavior throughout the dissipation and outflow regions, with frequencies reaching up to the electron cyclotron frequency.³⁰ Cai and Li study provides a systematic analysis of the dissipation mechanisms in reconnection and the pressure gradient effects on tearing mode with a guide magnetic field, finding

that which dissipation (i.e., pressure-based or inertia-based) mechanism dominates depends on the relative scaling orders between the electron thermal Larmor radius and electron inertia skin depth.³¹ In a series of recent studies within the EMHD regime, Jain et al. demonstrate that current disruption is an inherent aspect during the dynamic formation of an X-point magnetic field configuration in reconnection, irrespective of the plasma model or the reconnection's dimensionality (2D or 3D). Furthermore, they found that current disruption, induced by localized MR, propagates along the electron drift velocity direction at a speed determined by the perturbation's wave number.³² Subsequent research delved into the 3D instabilities of electron-scale current sheets in collisionless MR, by Jain and Büchner, revealing their crucial role in governing the efficiency and rate of reconnection processes.³³ Additionally, they examined the impact of guide fields on three-dimensional electron shear flow instabilities within electron current sheets. Their studies elucidated how guide fields modify the growth rates and characteristics of these instabilities.³⁴ This line of research by Jain et al., extended to electron acceleration and heating during guide field reconnection in EMHD turbulence, responsible for the particle energization processes.³⁵ Recently, Khabarova et al., identified electron-dominated current sheets in the collisionless turbulent solar wind by determining the electron-to-ion bulk speed ratio and found that electron-dominated current sheets are prevalent in the solar wind.³⁶

Gaur and Kaw, in the context of 2D EMHD, studied the susceptibility of electron current configurations to tearing and surface preserving instabilities when the equilibrium length scales are less than the ion skin depth.³⁷ Although both modes are driven due to equilibrium current-gradient, their evaluation is completely different. While the tearing mode leads to the formation of magnetic islands, the surface-preserving mode, on the other hand, preserves the surface of magnetic flux. Moreover, the tearing mode is a non-local mode while the surface-preserving mode is a local mode (unstable to the perturbations having wavelengths smaller than the equilibrium length scale). In this paper, we aim to study the kinetic effects of these two modes, such as the effect of temperature, and the interplay between temperature and the guide field. Fluid descriptions like EMHD break down at the kinetic scales, for instance, for hot plasmas or when the length scales are smaller than the gyroradius. Therefore, we have carried out particle-in-cell simulations to understand the linear and nonlinear stages of the two modes in the presence of kinetic effects.

The paper is organized as follows. In Section II, we discuss the basics of the particle-in-cell scheme along with the simulation setup we have used. In Section III, we present the results and discussions on various simulation runs we have conducted. In Section IV, we provide the conclusion.

II. PARTICLE-IN-CELL (PIC) METHOD AND SIMULATION SETUP

Particle simulation model can be classified into three principal types: the particle-particle (PP) model, the particle-mesh (PM) model, and the particle-particle-particle-mesh (PPPM or P3M) model.³⁸ The PP model utilizes the action-at-a-distance approach of the force law, the PM model implements the force as a field quantity (approximating it on a mesh), and the P3M model incorporates characteristics of both the PP and PM models."

The Particle-in-Cell (PIC) method is based on the PM model. In PIC simulations, the plasma is represented by a large number of superparticles, each representing a cluster of real particles, typically electrons and ions. These superparticles move through a computational grid (mesh) where the electromagnetic fields are calculated. The position and velocity of each particle are given as initial conditions, which determine the continuous distribution of the particles' position and velocity in space.

The PIC algorithm involves a self-consistent cycle: assigning charge to the mesh, solving Maxwell's equations and computing the fields from the mesh-defined potential, and updating the particle velocity and position based on the fields. Figure 1 shows the algorithm for the PIC technique, which includes the Boris scheme for pushing particles and a finite difference solver for the field calculations. There are various PIC codes available for plasma simulations; some of the widely used are VPIC (Vector Particle-In-Cell), iPIC3D, P3D, GEM (Geospace Environment Model) and OSIRIS.

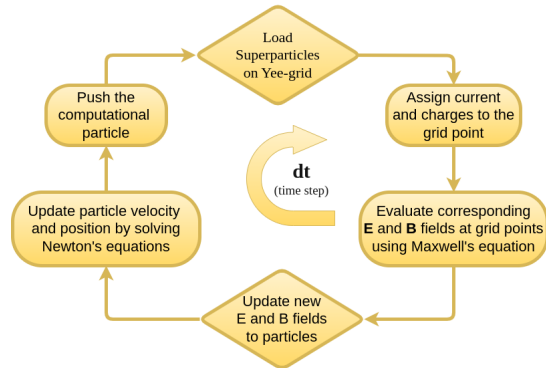


FIG. 1. PIC Algorithm

OSIRIS is a state-of-the-art PIC simulation code that is fully relativistic, massively parallel and fully object-oriented. Written in Fortran-90, it is designed for high-performance computing with multi-dimensional capabilities³⁹. OSIRIS simulates the behavior of plasmas by solving the Vlasov-Maxwell equations using the PIC method and is optimized for large-scale parallel supercomputers, utilizing the Message Passing Interface (MPI) for communication between processors⁴⁰.

Widely used in plasma physics research, OSIRIS features comprehensive physics models, including electromagnetic fields, relativistic particle dynamics, collisions, and radiation

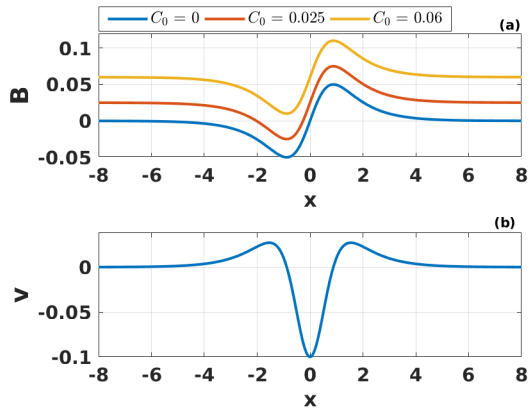


FIG. 2. (a) Equilibrium \mathbf{B} and (b) corresponding equilibrium \mathbf{v} profiles.

mechanisms. It excels in modeling complex plasma interactions, such as laser-plasma interactions for inertial confinement fusion⁴¹ and particle acceleration in astrophysical phenomena like magnetic reconnection, gamma-ray bursts, and relativistic jets⁴².

We have utilized the OSIRIS 4.0 framework⁴³ to model the 2D tearing and surface preserving instabilities. In our simulations, the normalized units are defined as follows: length is normalized by electron skin depth c/ω_{pe} , time is normalized by ω_{pe}^{-1} , and magnetic field by the quantity $\frac{m_e c^2}{e(c/\omega_{pe})}$. Where c is the speed of light, ω_{pe} is the electron plasma frequency, and m_e is the electron mass.

We have initialized our simulations for a thin current sheet equilibrium having width of the magnitude ε and z is the symmetry direction i.e., $(\frac{\partial}{\partial z}) = 0$. Ions are at rest (i.e., $v_i = 0$). Equilibrium magnetic field is expressed as follows:

$$\mathbf{B}_{eq} = \hat{y}B_0(x) = B_{00}\{sech(x/\varepsilon)tanh(x/\varepsilon)\} + C_0, \quad (1)$$

Corresponding equilibrium velocity is written as,

$$\begin{aligned} \mathbf{v}_{eq} (= -\nabla \times \mathbf{B}_{eq}) &= \hat{z}v_0(x) \\ &= \frac{B_{00} \sinh^2(x/\varepsilon)}{\varepsilon \cosh^3(x/\varepsilon)} \end{aligned} \quad (2)$$

Where, ε is shear width, B_{00} is the amplitude of the magnetic field, C_0 is a uniform magnetic field added externally in the direction of field.

In all our simulation runs, we have chosen $B_{00} = 1$ and $\varepsilon = 1$. A 2D rectangular simulation box with dimensions $L_x = 8(c/\omega_{pe})$ and $L_y = 3(c/\omega_{pe})$ has been chosen. The spatial resolution corresponds to a grid size of $\Delta x = 2L_x/512$ and $\Delta y = 2L_y/256$. A uniform plasma number density $n_0 = 10^{18}cm^{-3}$ has been chosen. We allow the equilibrium to evolve against the numerical perturbations. We have taken a periodic boundary conditions for both fields and particles because the equilibrium profile chosen is such that it ceases at both the boundaries. The equilibrium magnetic field and the corresponding equilibrium velocity profiles are shown in

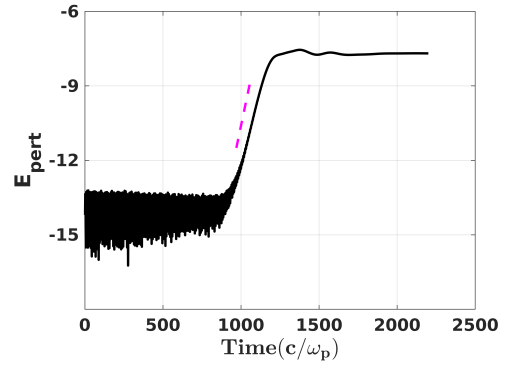


FIG. 3. The rate of evolution of perturbed energy obtained from the PIC simulation matches with the growth rate calculated from linear analysis under the EMHD model (dashed line) for the tearing mode at $T = 0$ eV.

Fig. 2. Three different magnetic field profiles corresponds to three different values of C_0 viz., 0, 0.025, 0.06.

III. RESULTS AND DISCUSSION

In this section we present and discuss the results from various simulation runs obtained by varying the C_0 (a uniform magnetic field applied along the equilibrium magnetic field) and T (temperature).

A. $C_0 = 0$: Only Tearing Mode Case

We first choose $T = 0$. This is the typical tearing instability case which has been studied by various authors in past using fluid as well as PIC simulations. We have (re)produced this run to validate our simulation setup. In Fig. 3 we have plotted the evolution of perturbation energy. The rate at which the perturbation energy grows matches well with the growth rate obtained from the linear instability calculations³⁷. In Fig. 4, the contours in the background depict the structure of the out-of-plane magnetic field. The magnetic field lines, superimposed on these contours, are straight, initially. However, as the tearing instability progresses, these field lines begin to bend, eventually forming an island structure. Concurrently, the out-of-plane magnetic field develops a distinctive quadrupolar pattern. These features are characteristic indicators of the tearing instability.

Having validated the simulation setup, we now proceed to study the effect of temperature on tearing instability. We conduct simulation runs for the following temperature values: ($T = 5, 10, 20, 50, 100, 200, 500, 1000$) electron volts. Upon increasing the temperature, while the characteristic features of the instability (such as the formation of islands and quadrupoles) remain more or less the same, we observe a variation in the growth rate with temperature. Fig. 5 illustrates the variation in the growth rate as temperature increases. The growth rate initially increases with temperature and then starts

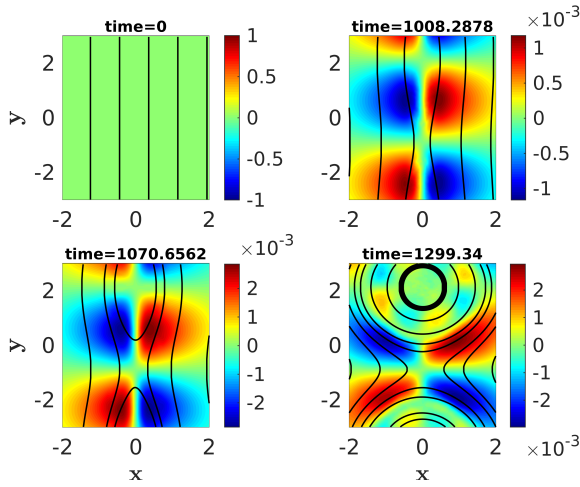


FIG. 4. Shaded isocontours of out-of-plane magnetic field with superimposed streamlines (solid lines) over various times for $C_0 = 0$ and $T = 0$ eV case.

decreasing monotonically. This behavior can be understood as follows.

Initially, when the temperature increases (say, up to 10 eV), the kinetic energy of the electrons increases. This makes the tearing instability more favorable, as the electrons move faster in the tearing instability plane compared to the case with $T = 0$. Consequently, the instability growth rate increases marginally. If the temperature further increases (beyond 10 eV), electron larmor radius (r_L) increases significantly, which is given as $r_L = v_{th}/\omega_{ce}$, where $v_{th} = \sqrt{p_e/(nm)}$ and $\omega_{ce} = eB/(m_e c)$ are the thermal velocity and plasma cyclotron frequency respectively. In other words, kinetic pressure starts dominating the the magnetic pressure i.e., the plasma beta (β) value increases, where $\beta = (n_e k_B T / (B^2 / 2\mu_0))$. This increases the diffusion of magnetic field (not just near the null-line) which, in turn, reduces the strength of current-gradient (due to weaker magnetic field and hence weaker current). As a result, the growth rate decreases. Eventually, at $T \geq 1keV$, the instability completely suppresses.

To reinforce our argument on the role of larmor radius in tearing growth rate against temperature, we add a uniform guide field⁴⁴ (in the direction perpendicular to the plane of tearing mode). Addition of guide field increases the magnetic pressure (energy) of the system. Owing to which, the decrease in the growth rate now start dropping at a higher temperature. Fig. 6 shows that as the guide field increases, the peak in the growth rate shift towards higher temperature.

B. $C_0 = 0.06$: Only Surface Preserving Mode Case

We now add C_0 , a uniform magnetic field along the direction of equilibrium magnetic field. We choose $C_0 = 0.06$, as this would make the condition $B_0 - B_0'' \leq 0$ for the existence of the tearing mode to be violated. Coincidentally, the opposite condition $B_0 - B_0'' > 0$ favors the existence of the surface preserving instability. Hence, only the surface preserving mode

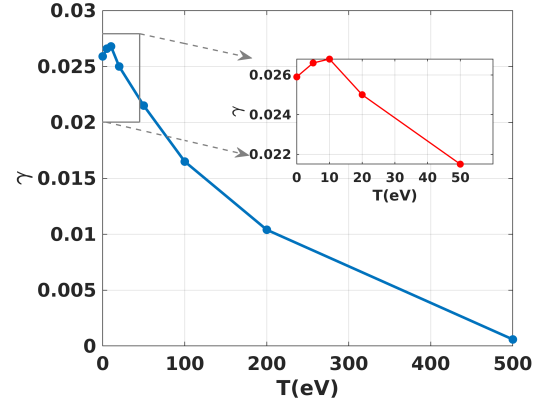


FIG. 5. The variation in growth rate calculated for the evolution of perturbed energy for $C_0 = 0$ case with temperatures (T) in eV . The inset figure highlights growth rate changes for $T = 0, 5, 10, 20$ and 50 eV

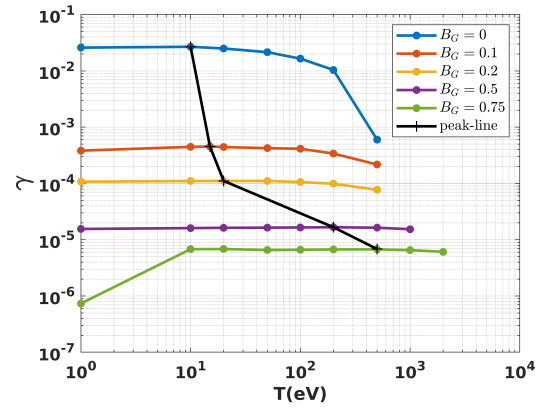


FIG. 6. Growth rate of perturbed energy evolution for $C_0 = 0$ with varying guide field values and temperatures. The black line denotes the peak value for each growth rate curve at different guide field values.

will be present in this case³⁷.

Simulation run with $T = 0$ eV, show no formation of quadrupoles or islands, which is unlike the tearing mode scenario. Magnetic field lines in this case do not bend and instead form a channel-like structure, as depicted in Fig. 7. In order to understand the behaviour of growth rate of surface preserving mode we conduct simulation runs for the following temperature values: ($T = 5, 10, 20, 50, 100, 200, 500$) electron volts. In Fig. 8, we plot the growth rate vs temperature. In this case, the growth rate goes on to increase, unlike the tearing mode case where the growth rate first increases and then start decreasing after a certain temperature. This can be explained as follows. Surface preserving mode, also termed as stationary nontearing inertial scale mode, is driven by the electron flow perturbations along the direction of the current gradient⁴⁵. An increase in temperature increases the electron flow velocity which, in turn, makes the instability more favourable.

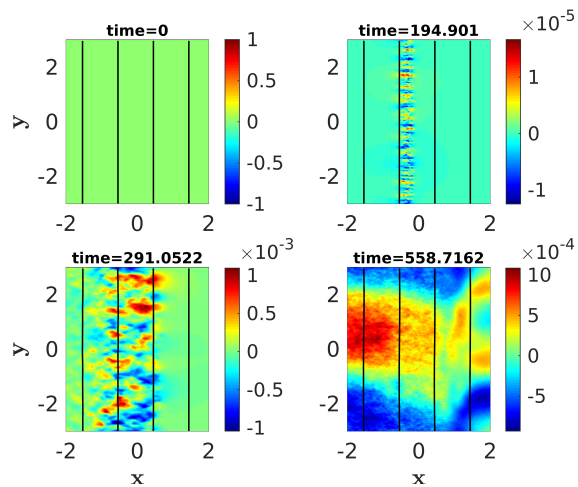


FIG. 7. Shaded isocontours of out-of-plane magnetic field with superimposed streamlines (solid lines) over various times for $C_0 = 0.06$ and $T = 0$ eV case.

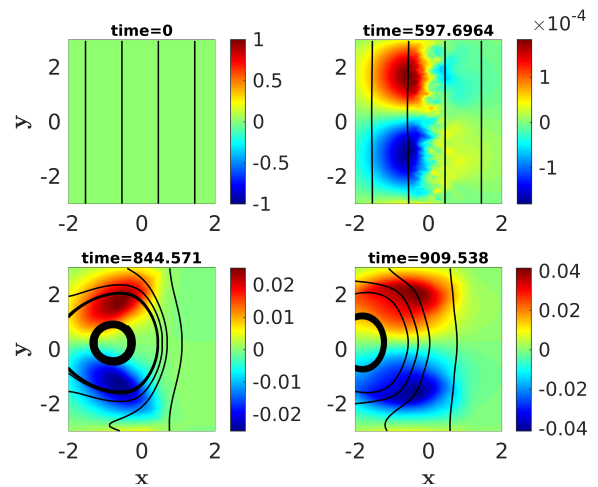


FIG. 9. Shaded isocontours of out-of-plane magnetic field with superimposed streamlines (solid lines) over various times for $C_0 = 0.025$ and $T = 0$ eV case.

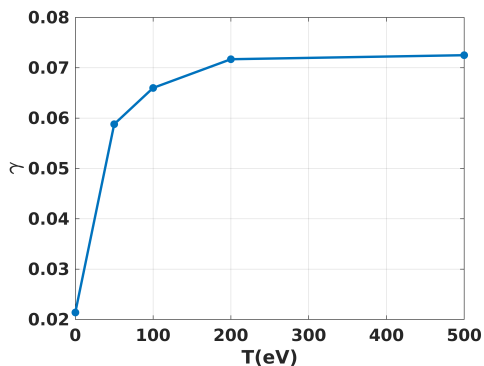


FIG. 8. The variation in growth rate calculated for the evolution of the perturbed energy of $C_0 = 0.06$ case with temperatures (T) in eV.

C. $C_0 = 0.025$: Mixed Modes Case

In this last case, we choose $C_0 = 0.025$. This value of C_0 permits both tearing and surface preserving modes to exist simultaneously. Due to the presence of tearing mode, the initially straight magnetic field lines evolve and then form an island. However, unlike the only tearing mode case (for $C_0 = 0$), the island formed in this case is asymmetric (see Fig. 9). The asymmetry is also observed in the evolution of out-of-plane magnetic field, the quadrupole formed is asymmetric.

Another interesting observation we made is that the island does not remain at its original location; it moves towards the left, the side with the weaker magnetic field. In Fig. 10, we see that initially the island forms at the null-line, denoted by a vertical line (at $x = -0.2661$), and it is asymmetric. As time progresses, the island shifts leftward. As seen in last subplot, the island has moved away from the vertical null-line. In contrast, in the case of only the tearing mode, a symmetric island forms at the null-line (at $x = 0.0$ in this case) and remains there, as shown in various subplots of Fig. 11. Shaded isocontours

of equilibrium current show the formation of mushroom-like patterns. Two jet-like electron flows emerge from the neighboring X -points, which are essentially the outflows from two adjacent reconnection sites. These flows collide at the center of the O -point and then move perpendicularly to impact the closed magnetic surfaces on opposite sides, creating the mushroom-like structures. In the mixed modes case, the two electron flows encounter different strengths of the magnetic field on either side of the null-point. The stronger magnetic field experiences less bending due to higher magnetic tension. The collision of electron flows with magnetic surfaces of unequal strengths results in a net momentum toward the left. This net momentum causes the island and other structures to move in the negative x -direction. The unequal magnetic field strength on the two sides of the null-line is also the reason behind the formation of asymmetric structures. Some of these features have been reported in studies on asymmetric magnetic reconnection, which has recently garnered significant interest.

To understand the role of temperature, we conducted simulation runs for the following temperature values: $T = 5, 10, 20, 50, 100, 200, 500$ electron volts. Figure 12 depicts the change in growth rate with temperature for this case. Similar to the case with only the tearing mode, the growth rate first increases with temperature and then starts decreasing. However, the peak of the curve has shifted to a lower temperature. Specifically, the peak growth rate occurs around 5 eV, compared to 10 eV in the only tearing mode case. The reason for this leftward shift of the peak is not certain at present. It could be due to asymmetry in the magnetic field on two sides of the null-line, the co-existence of the surface-preserving mode, and the effect of temperature on them. A more detailed study is underway to understand this effect.

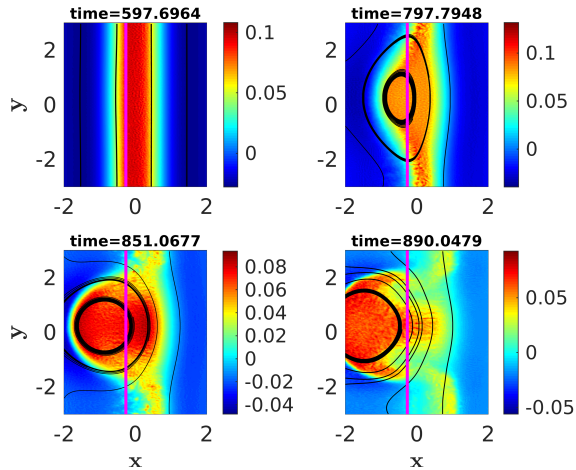


FIG. 10. Shaded isocontours of the current J_z with superimposed streamlines (black lines) over various times for $C_0 = 0.025$ and $T = 0$ eV case.

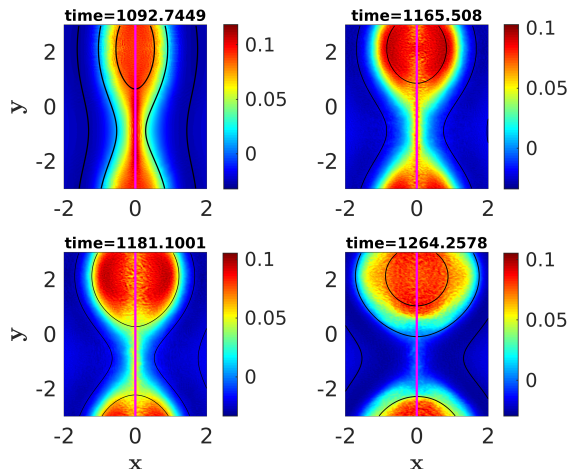


FIG. 11. Shaded isocontours of the current J_z with superimposed streamlines (black lines) over various times for $C_0 = 0$ and $T = 0$ eV case.

IV. SUMMARY AND FUTURE SCOPE

In this study, we conducted two-dimensional PIC simulations using the OSIRIS framework to investigate the kinetic effects on tearing and surface-preserving instabilities in electron current layers, which are relevant to various space, astrophysical, and laboratory plasma environments. We started by simulating the conventional tearing instability to validate our simulation setup. After validation, we explored the kinetic effects on the tearing mode by varying the electron temperature. Our results show that the growth rate of the tearing instability initially increased with temperature, peaking around 10 eV, before declining due to the increased electron Larmor radius and consequent diffusion of magnetic fields. To support our argument, we introduced a uniform guide field, which exhibited a stabilizing effect on the tearing mode, resulting in a shift

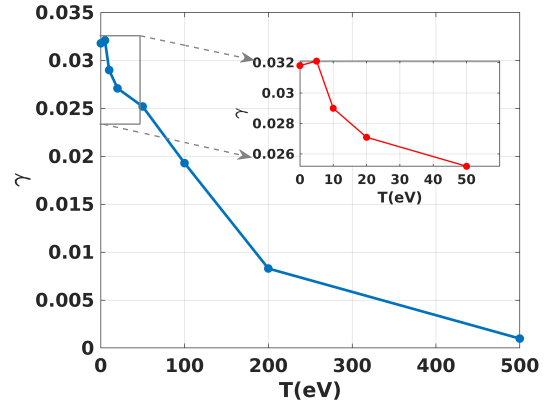


FIG. 12. The variation in growth rate calculated for the evolution of perturbed energy for $C_0 = 0.025$ case with temperatures (T) in eV. The inset figure highlights growth rate changes for $T = 0, 5, 10, 20$ and 50 eV

of the peak growth rate to higher temperatures.

To study the surface-preserving instability, we added a uniform magnetic field $C_0 = 0.06$ along the equilibrium magnetic field direction, which inhibits the tearing mode in the system. To analyze the effect of temperature on the growth rate of this mode, we ran simulations at various temperatures. The growth rate versus temperature plot shows a consistent rise, which can be attributed to the increased electron flow velocity at higher temperatures. This rise favors the instability, as it is driven by perturbations in the flow.

Finally, we also investigated the case when both the tearing and surface-preserving modes exist simultaneously in the system. Simulation runs in this scenario show that the structures (island and quadrupole) formed are asymmetric. Moreover, these structures do not remain stationary but move towards the weaker magnetic field side around the null-line. This behavior aligns with findings from studies on asymmetric magnetic reconnection. The growth rate's temperature dependence follows a pattern similar to the pure tearing mode case, initially increasing with temperature but peaking at lower temperature value. The causes of this shift are currently being studied, considering magnetic field asymmetries and the interplay between tearing and surface-preserving modes under varying temperatures.

Future Directions:

- In our studies, we have chosen the tanh - sech profile for the equilibrium magnetic field. While this allows us to use periodic boundary conditions, the profile naturally ceases at the boundaries. Conducting studies on larger systems (using profiles with a larger extent, such as the tanh profile) with appropriate boundary conditions (open or absorbing) provides a natural comparison. Comparing results from these larger systems with those from finite size systems would offer a more detailed understanding of the two modes.

- In our studies, we have chosen $\varepsilon = 1$, which is normalized by the electron skin depth. A parametric study by choosing $\varepsilon > 1$ (when the width of the current sheet is greater than the natural length scale - electron skin depth) and $\varepsilon < 1$ (when the width of the current sheet is smaller than the natural length scale) needs to be carried out to understand the behavior of the two modes in these different regimes, along with the role of temperature on their behavior.
- In mix modes cases, the magnetic field profile is not symmetric on two sides of the null-line. A separate study, by choosing the appropriate profiles, is required to separate the effect of asymmetry on the tearing mode and the interplay between the tearing and surface preserving modes. In only surface preserving mode case too, the strength of magnetic field is not equal. A magnetic profile with balanced strength will help in understating the evolution of surface preserving mode.
- Linear stability analysis using a warm EMHD (Electromagnetic Magnetohydrodynamics) model is currently underway and is essential for understanding the eigenmode structure under varying temperature conditions. This analysis will provide insights into how temperature influences the structure and stability of the modes.

ACKNOWLEDGMENTS

SM gratefully acknowledges the financial support provided by the Govt. of Gujarat under SHODH scheme. SM and GG would like to thank Professor Abhijit Sen for useful discussions.

- ¹M. Yamada, R. Kulsrud, and H. Ji, "Magnetic reconnection," *Reviews of modern physics* **82**, 603 (2010).
- ²R. Stenzel, M. Griskey, J. Urrutia, and K. Strohmaier, "Three-dimensional electron magnetohydrodynamic reconnection. i. fields, currents, and flows," *Physics of Plasmas* **10**, 2780–2793 (2003).
- ³R. Stenzel, M. Griskey, J. Urrutia, and K. Strohmaier, "Three-dimensional electron magnetohydrodynamic reconnection. iv. instabilities, fluctuations, and emissions," *Physics of Plasmas* **10**, 2810–2818 (2003).
- ⁴S. Bose, W. Fox, H. Ji, J. Yoo, A. Goodman, A. Alt, and M. Yamada, "Conversion of magnetic energy to plasma kinetic energy during guide field magnetic reconnection in the laboratory," *Physical Review Letters* **132**, 205102 (2024).
- ⁵P. A. Sweet, "The neutral point theory of solar flares," *Electromagnetic Phenomena in Cosmical Physics*, 123–134 (1958).
- ⁶E. N. Parker, "Sweet's mechanism for merging magnetic fields in conducting fluids," *Journal of Geophysical Research* **62**(4), 509–520 (1957).
- ⁷H. E. Petschek, "Magnetic field annihilation," *NASA Special Publication* **50**, 425 (1964).
- ⁸S. Bulanov, F. Pegoraro, and A. Sakharov, "Magnetic reconnection in electron magnetohydrodynamics," *Physics of Fluids B: Plasma Physics* **4**, 2499–2508 (1992).
- ⁹J. Birn and E. R. Priest, *Reconnection of magnetic fields: magnetohydrodynamics and collisionless theory and observations* (Cambridge University Press, 2007).
- ¹⁰M. A. Shay, J. F. Drake, R. E. Denton, and D. Biskamp, "Structure of the dissipation region during collisionless magnetic reconnection," *Journal of Geophysical Research: Space Physics* **103**, 9165–9176 (1998).
- ¹¹J. Drake, M. Shay, and M. Swisdak, "The hall fields and fast magnetic reconnection," *Physics of Plasmas* **15** (2008).
- ¹²D. Biskamp, "Magnetic reconnection in plasmas," *Astrophysics and Space Science* **242**, 165–207 (1996).
- ¹³A. P. Matthews, "Current advance method and cyclic leapfrog for 2d multi-species hybrid plasma simulations," *Journal of Computational Physics* **112**, 102–116 (1994).
- ¹⁴W. Daughton, V. Roytershteyn, B. Albright, H. Karimabadi, L. Yin, and K. J. Bowers, "Transition from collisional to kinetic regimes in large-scale reconnection layers," *Physical review letters* **103**, 065004 (2009).
- ¹⁵R. Horiuchi and T. Sato, "Three-dimensional particle simulation of plasma instabilities and collisionless reconnection in a current sheet," *Physics of Plasmas* **6**, 4565–4574 (1999).
- ¹⁶M. Mandt, R. Denton, and J. Drake, "Transition to whistler mediated magnetic reconnection," *Geophysical Research Letters* **21**, 73–76 (1994).
- ¹⁷B. Rogers, R. Denton, J. Drake, and M. Shay, "Role of dispersive waves in collisionless magnetic reconnection," *Physical Review Letters* **87**, 195004 (2001).
- ¹⁸X. Wang, A. Bhattacharjee, and Z. Ma, "Scaling of collisionless forced reconnection," *Physical review letters* **87**, 265003 (2001).
- ¹⁹J. Birn, J. Drake, M. Shay, B. Rogers, R. Denton, M. Hesse, M. Kuznetsova, Z. Ma, A. Bhattacharjee, A. Otto, *et al.*, "Geospace environmental modeling (gem) magnetic reconnection challenge," *Journal of Geophysical Research: Space Physics* **106**, 3715–3719 (2001).
- ²⁰J. D. Huba, "Hall magnetohydrodynamics-a tutorial," *Space Plasma Simulation*, 166–192 (2003).
- ²¹J. M. Dawson, "Particle simulation of plasmas," *Reviews of modern physics* **55**, 403 (1983).
- ²²L.-J. Chen, M. Hesse, S. Wang, D. Gershman, R. Ergun, J. Burch, N. Bessho, R. Torbert, B. Giles, J. Webster, *et al.*, "Electron diffusion region during magnetopause reconnection with an intermediate guide field: Magnetospheric multiscale observations," *Journal of Geophysical Research: Space Physics* **122**, 5235–5246 (2017).
- ²³M. Hesse, M. Kuznetsova, and M. Hoshino, "The structure of the dissipation region for component reconnection: Particle simulations," *Geophysical research letters* **29**, 4–1 (2002).
- ²⁴J. Drake, M. Swisdak, K. Schoeffler, B. Rogers, and S. Kobayashi, "Formation of secondary islands during magnetic reconnection," *Geophysical research letters* **33** (2006).
- ²⁵J. Dahlin, J. Drake, and M. Swisdak, "The role of three-dimensional transport in driving enhanced electron acceleration during magnetic reconnection," *Physics of Plasmas* **24** (2017).
- ²⁶W. Daughton, J. Scudder, and H. Karimabadi, "Fully kinetic simulations of undriven magnetic reconnection with open boundary conditions," *Physics of Plasmas* **13** (2006).
- ²⁷W. Daughton, V. Roytershteyn, H. Karimabadi, L. Yin, B. J. Albright, B. Bergen, and K. Bowers, "Role of electron physics in the development of turbulent magnetic reconnection in collisionless plasmas," *Nature Physics* **7**, 539–542 (2011).
- ²⁸K. Avinash, S. Bulanov, T. Esirkepov, P. Kaw, F. Pegoraro, P. Satorov, and A. Sen, "Forced magnetic field line reconnection in electron magnetohydrodynamics," *Physics of Plasmas* **5**, 2849–2860 (1998).
- ²⁹D. Del Sarto, F. Califano, and F. Pegoraro, "Current layer cascade in collisionless electron-magnetohydrodynamic reconnection and electron compressibility effects," *Physics of plasmas* **12** (2005).
- ³⁰J. Drake, M. Swisdak, H. Che, and M. Shay, "Electron acceleration from contracting magnetic islands during reconnection," *Nature* **443**, 553–556 (2006).
- ³¹H. Cai and D. Li, "Magnetic reconnection with pressure tensor in electron magnetohydrodynamics," *Physics of Plasmas* **16** (2009).
- ³²N. Jain, J. Büchner, S. Dorfman, H. Ji, and A. Surjalal Sharma, "Current disruption and its spreading in collisionless magnetic reconnection," *Physics of Plasmas* **20** (2013).
- ³³N. Jain and J. Büchner, "Three dimensional instabilities of an electron scale current sheet in collisionless magnetic reconnection," *Physics of Plasmas* **21** (2014).
- ³⁴N. Jain and J. Büchner, "Effect of guide field on three-dimensional electron shear flow instabilities in electron current sheets," *Journal of Plasma Physics* **81**, 905810606 (2015).
- ³⁵N. Jain, J. Büchner, and P. A. Muñoz, "Nonlinear evolution of electron shear flow instabilities in the presence of an external guide magnetic field," *Physics of Plasmas* **24** (2017).

- ³⁶O. Khabarova, J. Büchner, N. Jain, T. Sagitov, H. Malova, and R. Kislov, “Electron-to-ion bulk speed ratio as a parameter reflecting the occurrence of strong electron-dominated current sheets in the solar wind,” *The Astrophysical Journal* **933**, 97 (2022).
- ³⁷G. Gaur and P. K. Kaw, “Tearing and surface preserving electron magnetohydrodynamic modes in a current layer,” *Physics of Plasmas* **23** (2016).
- ³⁸R. W. Hockney and J. W. Eastwood, *Computer simulation using particles* (crc Press, 2021).
- ³⁹R. Fonseca, L. Silva, F. Tsung, V. Decyk, W. Lu, C. Ren, W. Mori, S. Deng, S. Lee, T. Katsouleas, *et al.*, “Lecture notes in computer science,” *Lecture Notes in Computer Science* **2331**, 342–351 (2002).
- ⁴⁰R. A. Fonseca, J. Vieira, F. Fiúza, A. Davidson, F. S. Tsung, W. B. Mori, and L. O. Silva, “Exploiting multi-scale parallelism for large scale numerical modelling of laser wakefield accelerators,” *Plasma Physics and Controlled Fusion* **55**, 124011 (2013).
- ⁴¹A. Kemp, F. Fiúza, A. Debayle, T. Johzaki, W. Mori, P. Patel, Y. Sentoku, and L. Silva, “Laser–plasma interactions for fast ignition,” *Nuclear Fusion* **54**, 054002 (2014).
- ⁴²L. O. Silva, R. Fonseca, J. Tonge, J. Dawson, W. Mori, and M. Medvedev, “Interpenetrating plasma shells: near-equipartition magnetic field generation and nonthermal particle acceleration,” *The Astrophysical Journal* **596**, L121 (2003).
- ⁴³R. Fonseca, T. Dalichaouch, A. Davidson, F. Cruz, F. Del Gaudio, G. Inchingolo, A. Helm, R. Lee, F. Li, J. May, *et al.*, “Osiris 4.0: A state of the art framework for kinetic plasma simulations,” in *APS Division of Plasma Physics Meeting Abstracts*, Vol. 2018 (2018) pp. PP11–023.
- ⁴⁴Presence of a guide field is known to play a stabilizing role in magnetic reconnection.
- ⁴⁵V. Lukin, “Stationary nontearing inertial scale electron magnetohydrodynamic instability,” *Physics of Plasmas* **16** (2009).